# DOUBLE LAYERED COMPRESSIBLE MASKS

N. D. FOWKES[1] and D. P. MASON[2]

## Abstract

Double-masking may be used to reduce the transmission of a virus. If additionally the masks are compressible, with different permeabilities and behaviour under compression, then it may be possible to design a mask that allows for easy breathing under normal breathing conditions, but is relatively impermeable under coughing or sneezing conditions. Such a mask could be both comfortable to wear and effective. We obtain analytical solutions for the steady-state flow-through behaviour of such a double mask under flow-out conditions. The results show that the reduction in permeability required to produce a relatively impermeable mask under high flux expulsion (sneezing) conditions could be achieved using either a single filter compressible mask or two filters with different poroelastic parameters. The parameters can be more easily adjusted using a double mask. For both single- and double-mask cases, there is an abrupt cut off, whereby through-flux levels reduce from a maximum value to zero as pressure drop levels increase beyond a critical value. Additionally, in the double-mask case, there exists a second steady-state solution for particular parameter ranges. This second solution is unlikely to occur under normal circumstances.

## 1. Introduction

There is considerable interest in the use of masks to reduce the spread of COVID-19. In many countries, the wearing of a mask is compulsory in public places. Most of the masks in use are one filter layer masks. Dr Fauci, who is the Director of the United States National Institute of Allergy and Infectious Diseases, recently advised:

---

[1]School of Mathematics and Statistics, University of Western Australia, Western Australia, Australia; e-mail: neville.fowkes@uwa.edu.au

[2]School of Computational and Applied Mathematics, University of the Witwatersrand, Johannesburg, South Africa; e-mail: David.Mason@wits.ac.za

"If you have a physical covering with one layer, you put another layer on, it just makes common sense that it likely would be more effective. That is the reason why you see people either use double masking or doing a version of an N-95" [2]. The MISG in South Africa was asked to contribute to the understanding of the effects of masks on the spread of infectious respiratory droplets as in COVID-19. One subgroup focused on the effect of mask design (fitting accuracy, mask design, air permeability of the filter) on the through-flow verses leakage flow behaviour of the mask [3]. The second subgroup investigated the effect of "double masking" on the through-flow behaviour. The mask could consist of either a mask made of two filter layers with different material properties or two masks in perfect contact with no air gap between the masks. The results obtained by this subgroup are the subject of this article.

Many filters in use can be described as being incompressible in the sense that the permeability (and porosity) of such filters remains constant irrespective of the applied pressure drop and accompanying flow through them. By virtue of the difference in porosity between the two layers making up a double mask, there can be improved performance, because the two layers can filter out different size particles. Typically, the filter/mask closer to the face could be used to capture larger particles, with smaller particles being captured in the outer filter/mask. However, filters may be compressible in the sense that the permeability (and porosity) changes with applied pressure and this affects the flow-through as well as particle capture [5, 7]. Such compressibility effects may be advantageous when designing a double mask. The subgroup considered two compressible masks in which the permeability depends linearly on the deformation gradient of the mask. This article will focus on the fluid flow through the mask/s. A later article will address the associated porosity/particle capture aspects of the problem.

The structure of the paper is as follows. In Section 2, the model equations for the double compressible masks are presented. A poroelastic model [4] is used to describe the flow through the masks; a brief review of this model is presented in Section 2.1. Analytic solutions of the model equations are obtained in Section 3. Two subsections are included to massage the results into a suitable form for presentation and interpretation. The compressible double masks results are presented in Section 4. The simpler incompressible double masks case results are relegated to Appendix A. Finally, conclusions are drawn in Section 5. Note that colours for all figures are available online.

**1.1. Previous work**   Face masks have been used for centuries to provide protection from pollutants and pathogens, but attempts to understand the physics of the flow and the filtration physics in this context are more recent, with an enormous increase in activity since the advent of the COVID-19 pandemic. The associated fluid dynamics is complicated involving, as it does, scales varying from nanometres (fibre diameter) to metres (the distance travelled by a respiratory jet), with structural dynamics, droplet and particle dynamics, and even electrostatics playing a role [8]. Computational mask flow experiments have been undertaken using real world observations [1].

A flood of mask types have entered the market broadly classified as being fixed facepiece masks (including N95 masks), medical and surgical masks, and cloth masks using either woven or unwoven fabrics. Permeability results are available for mask materials, largely coming out of the textile industry [6]. A recent review of the fluid dynamics-centric materials can be found in the work of Rajat et al. [8]. The work presented in the current paper involves flow through a compressible filter which was studied by Köry et al. [5] in the context of industrial filtering.

## 2.  The two-layer compressible mask model

A two-layer mask could consist either of two masks in perfect contact with no air gap between them, or a mask made of two layers of different material. A model of a two-layer compressible mask is illustrated in Figure 1. It is assumed that the mask can be represented by a one-dimensional model. The outer mask (Mask 1 or layer 1) extends in the range $0 \leq x \leq L_1$, while the inner mask (Mask 2 or layer 2) is of width $L_2$ and extends in the range $L_1 \leq x \leq L$, where $L = L_1 + L_2$. There is an effective porous grid attached to the outer face $x = 0$ of Mask 1, which is held in position by the mask belt that extends around the head of the wearer. Fluid can flow through the porous grid without resistance. An imposed pressure difference across the masks, $\Delta P = P_{\text{in}} - P_{\text{out}}$ (where $P_{\text{in}}$ is the pressure at the mouth of the wearer at $x = L$ and $P_{\text{out}}$ is the pressure at the porous grid at $x = 0$) drives flow through the masks. The aim is to determine the resulting through-flux under steady-state conditions as a function of the poroelastic and thickness parameters of the masks. The mask will be modelled as an elastic matrix containing small pores which are connected and so allow the flow of viscous fluid through the mask. Poroelasticity is an appropriate setting for this work and so, before proceeding with the main text, we will give a brief review of the work in this area [4].

*Model applicability* The effect of a cough or sneeze is to inject air into the space between the mask and the face. The resultant pressure increase will cause air (with droplets) to pass through the mask filter/s, or leak out around the sides of the mask. The leakage versus mask through-flow problem is not addressed here (see however [3]). Here, we focus on the through flow brought about by the pressure drop across the filter/s. The timespan for a cough or sneeze is approximately 0.1 s [1] and the time span for mask deflation is largely determined by the leakage flow, because the filters offer more resistance to flow. Estimates typically give about 0.3 s or greater for the mask deflation time. During this time, the pressure drop will marginally vary with location within the mask but a one-dimensional (1D) model should provide a good estimate of filter performance in the mask context. The above time scales are very much greater than the transition time scale for flow through the mask/s (approximately $0.2 \times 10^{-5}$ s), so a (quasi) steady-state 1D model has been adopted.

### 2.1.  Poroelasticity   The net stress tensor in a poroelastic medium containing moving fluid is the sum of an elastic stress tensor in the solid matrix and the stress tensor in
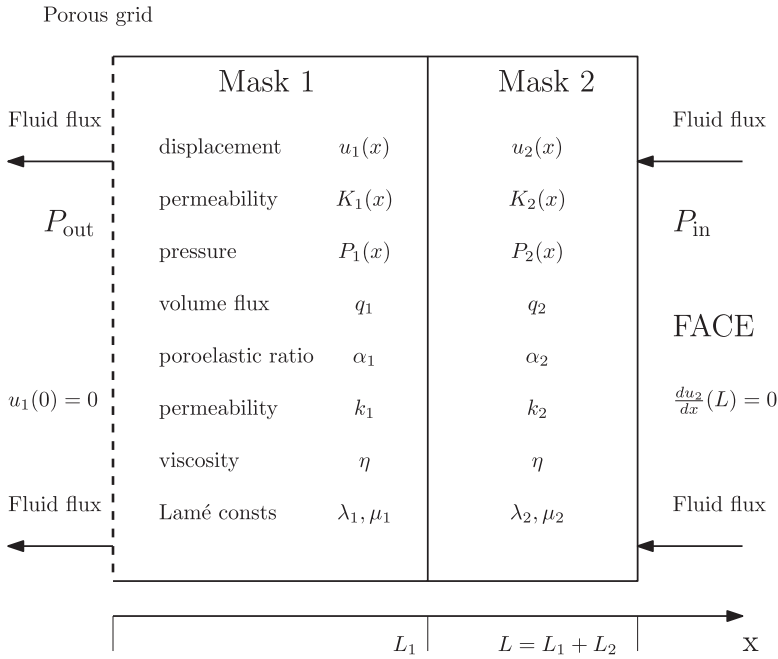
Porous grid



FIGURE 1. Two-layer compressible mask model. The outer mask (Mask 1 or layer 1) extends from $x = 0$ to $x = L_1$ and is joined to the inner mask (Mask 2 or layer 2) which extends from $x = L_1$ to the face at $x = L_1 + L_2$. The pressure drop $\Delta P = (P_{\text{in}} - P_{\text{out}}) > 0$ across the masks drives a volume flux $-q_1 = -q_2$ through the masks.

the fluid. We assume here that the medium is isotropic and homogeneous. The elastic contribution to the stress tensor in Cartesian coordinates $(x_1, x_2, x_3)$ is

$$\tau_{ik}^e = \lambda_{\text{eff}} \left( \boldsymbol{\nabla} \cdot \mathbf{u} \right) \delta_{ik} + 2 \mu_{\text{eff}} E_{ik}, \tag{2.1}$$

where $\mathbf{u}$ is the displacement vector, $\boldsymbol{\nabla}$ is the del vector operator and $E_{ik}$ is the strain tensor

$$E_{ik} = \frac{1}{2} \left( \frac{\partial u_i}{\partial x_k} + \frac{\partial u_k}{\partial x_i} \right).$$

The effective Lamé constants, $\lambda_{\text{eff}}$ and $\mu_{\text{eff}}$ are different from the Lamé constants of the material of the matrix. It is assumed that the stress in the fluid averages, on a length scale of many pore sizes, to an isotropic pore fluid pressure $P$ with stress tensor

$$\tau_{ik}^f = -P \, \delta_{ik}.$$

The net stress tensor of the porous elastic medium is therefore

$$\tau_{ik} = \tau_{ik}^e + \tau_{ik}^f = (-P + \lambda_{\text{eff}} \, \boldsymbol{\nabla} \cdot \mathbf{u}) \delta_{ik} + \mu_{\text{eff}} \left( \frac{\partial u_i}{\partial x_k} + \frac{\partial u_k}{\partial x_i} \right); \tag{2.2}$$

the inertia and body force terms due to gravity are neglected. Under steady conditions, the net stress tensor satisfies the equations of static equilibrium

$$\frac{\partial}{\partial x_k}\, \tau_{ki} = 0, \quad i = 1, 2, 3. \tag{2.3}$$

Substituting (2.2) into (2.3) leads to the Navier displacement equation for static equilibrium

$$\mu_{\text{eff}} \nabla^2 \mathbf{u} + (\lambda_{\text{eff}} + \mu_{\text{eff}})\, \boldsymbol{\nabla}(\boldsymbol{\nabla} \cdot \mathbf{u}) = \boldsymbol{\nabla} P. \tag{2.4}$$

The fluid flux $\mathbf{q}$ is the volume flow rate per unit surface area through the porous medium. Under the steady-state conditions of interest here, Darcy's law applies so that

$$\mathbf{q} = -\frac{K}{\eta}\, \boldsymbol{\nabla} P, \tag{2.5}$$

where $\eta$ is the viscosity of the fluid and $K$ is the permeability of the medium. Additionally, we need to impose mass conservation for the fluid which, under steady-state conditions (and neglecting fluid compressibility) gives

$$\boldsymbol{\nabla} \cdot \mathbf{q} = 0. \tag{2.6}$$

Poroelastic theory [4] takes into account the effect of solid matrix compressibility on the flow through the matrix, and assumes that the permeability depends on the displacement gradient [5, 7], so that, assuming a linear constitutive equation and a one-dimensional displacement $u(x)$, we write

$$K = k + \alpha_n^* \frac{du}{dx}, \tag{2.7}$$

where $k$ is the permeability of the material in its undeformed state. The poroelastic parameter $\alpha^*$ is assumed to be positive (or zero) for the mask situation of interest here, so that the permeability reduces as the material compresses. The elastic constants $\lambda_{\text{eff}}, \mu_{\text{eff}}$ and $\eta$ are assumed to remain constant. Note that the elastic and fluid flow equations are coupled in the poroelastic model.

The effect of compression is to change the pore size in the matrix which is closely related to the porosity, $\phi$, of the medium. An example of the relationship used in practice is the Kozeney–Carman equation

$$K = \frac{K_0 \phi^3}{(1 - \phi)^2}, \quad \frac{dK}{d\phi} = \frac{K_0(3 - \phi)\phi^2}{(1 - \phi)^3}, \quad 0 < \phi < 1,$$

according to which the permeability is an increasing function of $\phi$. Whilst porosity is a major factor for determining particle capture, we will not be addressing this issue in this paper, so we will not need to impose a specific constitutive equation between the permeability and the porosity; it suffices to work directly with permeabilities.

**2.2. The model equations** We return to the double-mask problem (see Figure 1). Since the model is assumed to be one-dimensional, all quantities depend only on $x$. The quantities of Mask 1 are denoted by suffix 1 and Mask 2 by suffix 2. Thus,

$$\mathbf{u}_n = (u_n(x), 0, 0), \quad P_n = P_n(x), \quad n = 1, 2.$$

We take the fluid flux to be positive in the negative $x$-direction so that the fluid flux from the mouth and nose into the mask is positive. Hence,

$$\mathbf{q}_n = (-q_n(x), 0, 0), \quad n = 1, 2, \tag{2.8}$$

where $q_n(x) \geq 0$. To simplify the notation, $\lambda_{\text{eff}}$ and $\mu_{\text{eff}}$ will be denoted by $\lambda$ and $\mu$, respectively. Since the same fluid flows through both masks, the fluid viscosity is denoted simply by $\eta$.

Only the $x$-components of the equations of poroelasticity are not identically zero. The $x$-component of the Navier displacement equation (2.4) in each layer is

$$(\lambda_n + 2\mu_n) \frac{d^2 u_n}{dx^2} = \frac{dP_n}{dx}, \quad n = 1, 2. \tag{2.9}$$

The $x$-component of Darcy's law, (2.5), is

$$q_n(x) = \frac{K_n}{\eta} \frac{dP_n}{dx}, \quad n = 1, 2. \tag{2.10}$$

The permeability of the mask materials is assumed to depend linearly on the displacement gradient $du/dx$. So we have from (2.7)

$$K_n = k_n + \alpha_n^* \frac{du_n}{dx}, \quad n = 1, 2,$$

where $k_n$ is the permeability of the medium in its undeformed state and is a positive constant, and we have assumed that the constant $\alpha_n^* \geq 0$. We write

$$K_n = k_n \left( 1 + \alpha_n \frac{du_n}{dx} \right), \tag{2.11}$$

where $\alpha_n = \alpha_n^*/k_n$, which we will refer to as the "poroelastic ratio". This ratio is dimensionless and is a suitable small perturbation parameter to determine compressibility effects since for the rigid mask, $\alpha_n = 0$. Equation (2.10) becomes

$$q_n(x) = \frac{k_n}{\eta} \left( 1 + \alpha_n \frac{du_n}{dx} \right) \frac{dP_n}{dx}. \tag{2.12}$$

The conservation of mass equation (2.6) reduces to

$$\frac{dq_n}{dx} = 0, \quad n = 1, 2. \tag{2.13}$$

Next, we consider the boundary conditions. Mask 1 is attached to a porous grid at $x = 0$. The displacement at $x = 0$ must therefore be zero:

$$u_1(0) = 0. \tag{2.14}$$

At $x = L$, the end is not compressed and therefore is free of applied stress. Thus, from (2.1),

$$\tau_{xx}^e(L) = (\lambda_2 + 2\mu_2)\, \frac{du_2}{dx}\, (L) = 0. \tag{2.15}$$

The pressure at $x = 0$ and $x = L$ is $P_{\text{out}}$ and $P_{\text{in}}$ which are constants. Hence,

$$P_1(0) = P_{\text{out}}, \quad P_2(L) = P_{\text{in}}. \tag{2.16}$$

The pressure $P_{\text{in}}$ is prescribed, but we will see that the fluid flux and the pressure $P_{\text{out}}$ cannot both be prescribed.

Finally, there are matching conditions at the interface between the masks at $x = L_1$. We assume that the two masks are in perfect contact, and therefore at $x = L_1$, the displacement is continuous, so

$$u_1(L_1) = u_2\,(L_1), \tag{2.17}$$

and the fluid flux is continuous, so

$$q_1(L_1) = q_2\,(L_1). \tag{2.18}$$

The normal elastic stress is also continuous at $x = L_1$,

$$\tau_{xx}^e\,(L_1-) = \tau_{xx}^e(L_1+), \tag{2.19}$$

which, from (2.1), gives the matching condition

$$(\lambda_1 + 2\mu_1)\, \frac{du_1}{dx}\, (L_1) = (\lambda_2 + 2\mu_2)\, \frac{du_2}{dx}\, (L_1). \tag{2.20}$$

Since the stress in the fluid is continuous at $x = L_1$, the pore fluid pressure is continuous. Hence,

$$P_1(L_1) = P_2(L_1). \tag{2.21}$$

We will be interested in the flow for which $P_{\text{in}} > P_{\text{out}}$. The mask is then under compression since the porous grid is fixed at $x = 0$. The fluid flows in the negative $x$-direction and the $x$-component of the fluid flux in (2.8), $q_n(x)$, is positive. The model also applies for $P_{\text{out}} > P_{\text{in}}$.

The problem is to solve the six equations (2.9), (2.12) and (2.13) for the six quantities $u_n(x)$, $P_n(x)$ and $q_n(x)$, where $n = 1$ and 2, subject to the boundary conditions (2.14), (2.15) and (2.16), and the matching conditions (2.17), (2.18), (2.20) and (2.21).

We do not make the equations dimensionless, because we find that the solution can be expressed in terms of the ratios of $\alpha$, $k$ and $\lambda + 2\mu$ in the two layers.

## 3. Analytic solutions

We first detail the solution process in Section 3.1. The results are however complicated both in solution form and also because of the many parameter combinations occurring, so further processing is required to reduce the results to a form suitable for plotting and interpretation (Sections 3.2, 3.3 and 3.4).

**3.1. Solution extraction** From (2.13),

$$q_n(x) = q_{n0}, \quad n = 1, 2,$$

where $q_{n0}$ is a constant. However, from the matching condition (2.18),

$$q_{10} = q_{20} = q_0,$$

where $q_0$ is a constant.

Equation (2.12) becomes

$$\frac{dP_n}{dx} = \frac{q_0 \eta}{k_n} \left[ 1 + \alpha_n \frac{du_n}{dx} \right]^{-1}, \tag{3.1}$$

and by inserting (3.1) into (2.9), we obtain for $u_n$ the second-order differential equation

$$\frac{d^2 u_n}{dx^2} + \alpha_n \frac{du_n}{dx} \frac{d^2 u_n}{dx^2} = \frac{q_0 \eta}{k_n(\lambda_n + 2\mu_n)}. \tag{3.2}$$

Equation (3.2) can be rewritten as

$$\frac{d^2 u_n}{dx^2} + \frac{\alpha_n}{2} \frac{d}{dx}\left(\left(\frac{du_n}{dx}\right)^2\right) = \frac{q_0 \eta}{k_n(\lambda_n + 2\mu_n)},$$

and by integrating with respect to $x$, we obtain

$$\frac{\alpha_n}{2} \left(\frac{du_n}{dx}\right)^2 + \frac{du_n}{dx} - \left(A_n + \frac{q_0 \eta}{k_n(\lambda_n + 2\mu_n)} x\right) = 0, \tag{3.3}$$

where $A_n$ is a constant. Equation (3.3) is a quadratic equation for $du_n/dx$. Hence,

$$\frac{du_n}{dx} = -\frac{1}{\alpha_n} \pm \frac{1}{\alpha_n} \left[ 1 + 2\alpha_n \left(A_n + \frac{q_0 \eta}{k_n(\lambda_n + 2\mu_n)} x\right) \right]^{1/2}. \tag{3.4}$$

To decide which sign to take in (3.4), we expand (3.4) for small values of $\alpha_n$ and compare with the corresponding result for a rigid two-layer mask. Now,

$$\frac{du_n}{dx} = -\frac{1}{\alpha_n} \pm \frac{1}{\alpha_n} \pm \left(A_n + \frac{q_0 \eta}{k_n(\lambda_n + 2\mu_n)} x\right) + O(\alpha) \quad \text{as } \alpha \to 0. \tag{3.5}$$

However, for a rigid mask, $\alpha_n = 0$ and solving in the same way as for a compressible mask, we find that, instead of (3.5),

$$\frac{du_n}{dx} = A_{0n} + \frac{q_0 \eta}{k_n(\lambda_n + 2\mu_n)} x,$$

where $A_{0n}$ is a constant. By letting $\alpha_n \to 0$ in (3.5), we see that the "+" sign must be taken in (3.4). The constant $A_n$ could depend on $\alpha_n$, but in such a way that it tends to the finite constant $A_{0n}$ as $\alpha_n \to 0$. Equation (3.4) becomes

$$\frac{du_n}{dx} = -\frac{1}{\alpha_n} + \frac{1}{\alpha_n}\left[ 1 + 2\alpha_n \left(A_n + \frac{q_0 \eta}{k_n(\lambda_n + 2\mu_n)} x\right) \right]^{1/2}, \tag{3.6}$$

and by integrating again, we obtain for the displacement

$$u_n(x) = -\frac{x}{\alpha_n} + \frac{k_n(\lambda_n + 2\mu_n)}{3\,\alpha_n^2\,q_0\,\eta}\left[1 + 2\alpha_n\left(A_n + \frac{q_0\,\eta}{k_n(\lambda_n + 2\mu_n)}\,x\right)\right]^{3/2} + B_n, \qquad (3.7)$$

where $B_n$ is a constant.

The pressure in the fluid, $P_n(x)$, is obtained by substituting (3.6) into (3.1). This gives

$$\frac{dP_n}{dx} = \frac{q_0\,\eta}{k_n}\left[1 + 2\alpha_n\left(A_n + \frac{q_0\,\eta}{k_n(\lambda_n + 2\mu_n)}\,x\right)\right]^{-1/2},$$

and by integrating with respect to $x$, we obtain

$$P_n(x) = \frac{(\lambda_n + 2\mu_n)}{\alpha_n}\left[1 + 2\alpha_n\left(A_n + \frac{q_0\eta}{k_n(\lambda_n + 2\mu_n)}\,x\right)\right]^{1/2} + C_n, \qquad (3.8)$$

where $C_n$ is a constant.

We now apply the boundary conditions. Imposing the boundary conditions (2.14) on (3.7), (2.15) on (3.6) and the first condition in (2.16) on (3.8) gives

$$\frac{k_1(\lambda_1 + 2\mu_1)}{3\alpha_1^2\,q_0\,\eta}\,(1 + 2\alpha_1\,A_1)^{1/2} + B_1 = 0, \qquad (3.9)$$

$$A_2 = -\frac{q_0\,\eta\,L}{k_2(\lambda_2 + 2\mu_2)}, \qquad (3.10)$$

$$\frac{(\lambda_1 + 2\mu_1)}{\alpha_1}\,(1 + 2\alpha_1\,A_1)^{1/2} + C_1 = P_{\text{out}}. \qquad (3.11)$$

Imposing the second pressure boundary condition in (2.16) on (3.8) and using (3.10) gives

$$C_2 = P_{\text{in}} - \frac{(\lambda_2 + 2\mu_2)}{\alpha_2}. \qquad (3.12)$$

It remains to impose the matching conditions at the interface $x = L_1$. By using (3.7) for $u_n(x)$ and replacing $A_2$ in terms of $q_0$ by (3.10), the matching condition (2.17) becomes

$$-\frac{L_1}{\alpha_1} + \frac{k_1(\lambda_1 + 2\mu_1)}{3\alpha_1^2\,q_0\,\eta}\left[1 + 2\alpha_1\left(A_1 + \frac{q_0\,\eta\,L_1}{k_1(\lambda_1 + 2\mu_1)}\right)\right]^{3/2} + B_1$$

$$= -\frac{L_1}{\alpha_2} + \frac{k_2(\lambda_2 + 2\mu_2)}{3\alpha_2^2\,q_0\,\eta}\left[1 - \frac{2\alpha_2\,q_0\,\eta(L - L_1)}{k_2(\lambda_2 + 2\mu_2)}\right]^{3/2} + B_2. \qquad (3.13)$$

By using (3.6) and eliminating $A_2$ with (3.10), the matching condition (2.20) becomes

$$(\lambda_1 + 2\mu_1)\left[-\frac{1}{\alpha_1} + \frac{1}{\alpha_1}\left[1 + 2\alpha_1\left(A_1 + \frac{q_0\,\eta\,L_1}{k_1(\lambda_1 + 2\mu_1)}\right)\right]^{1/2}\right]$$

$$= (\lambda_2 + 2\mu_2)\left[-\frac{1}{\alpha_2} + \frac{1}{\alpha_2}\left[1 - \frac{2\alpha_2\,q_0\,\eta(L - L_1)}{k_2(\lambda_2 + 2\mu_2)}\right]^{1/2}\right]. \qquad (3.14)$$

The remaining matching condition (2.21) becomes, using (3.8) for $P_n(x)$, (3.10) for $A_2$ and (3.12) for $C_2$,

$$\frac{(\lambda_1 + 2\mu_1)}{\alpha_1}\left[1 + 2\alpha_1\left(A_1 + \frac{q_0\,\eta_1\,L_1}{k_1(\lambda_1 + 2\mu_1)}\right)\right]^{1/2} + C_1$$

$$= \frac{(\lambda_2 + 2\mu_2)}{\alpha_2}\left[1 - \frac{2\alpha_2\,q_0\,\eta(L - L_1)}{k_2(\lambda_2 + 2\mu_2)}\right]^{1/2} - \frac{(\lambda_2 + 2\mu_2)}{\alpha_2} + P_{\text{in}}. \qquad (3.15)$$

There are eight quantities, $A_1$, $B_1$, $C_1$, $A_2$, $B_2$, $C_2$, $q_0$ and $P_{\text{out}}$, and there are seven equations, (3.9)–(3.15). Since $P_{\text{in}}$ is prescribed, the constant $C_2$ is given by (3.12). The constant $A_2$ is determined in terms of $q_0$ from (3.10), while $A_1$ is determined in terms of $q_0$ from the matching condition (3.14). With $A_1$ determined in terms of $q_0$, $B_1$ and $C_1$ are obtained in terms of $q_0$ from (3.9) and (3.15), while $B_2$ is now obtained in terms of $q_0$ from (3.13). Since $A_1$ and $C_1$ can be expressed in terms of $q_0$, the remaining boundary condition (3.11) is a relation between $q_0$ and $P_{\text{out}}$. The fluid flux $q_0$ and the exit pressure $P_{\text{out}}$ cannot both be prescribed. Either $q_0$ or $P_{\text{out}}$ is prescribed. The quantity not prescribed is then determined from (3.11).

Where possible, the constants are expressed in terms of the ratio of the parameters in the two masks. The following results are obtained for the constants:

$$A_1 = -\frac{q_o\,\eta\,L_1}{k_1(\lambda_1 + 2\mu_1)} - \frac{1}{2\alpha_1}$$
$$+ \frac{1}{2\alpha_1}\left[1 - \frac{\alpha_1}{\alpha_2}\left(\frac{\lambda_2 + 2\mu_2}{\lambda_1 + 2\mu_1}\right)\left\{1 - \left(1 - \frac{2\alpha_2\,q_0\,\eta\,L_2}{k_2(\lambda_2 + 2\mu_2)}\right)^{1/2}\right\}\right]^2, \qquad (3.16)$$

$$C_1 = P_{\text{in}} - \frac{(\lambda_1 + 2\mu_1)}{\alpha_1}, \qquad (3.17)$$

$$B_1 = -\frac{k_1(\lambda_1 + 2\mu_1)}{3\alpha_1^2\,q_0\,\eta}\,(1 + 2\alpha_1 A_1)^{3/2}, \qquad (3.18)$$

$$B_2 = L_1\left(\frac{1}{\alpha_2} - \frac{1}{\alpha_1}\right) + \frac{k_1(\lambda_1 + 2\mu_1)}{3\alpha_1^2 q_0\eta}\left[\left(1 + 2\alpha_1 A_1 + \frac{2\alpha_1 q_0\eta L_1}{k_1(\lambda_1 + 2\mu_1)}\right)^{3/2} - (1 + 2\alpha_1 A_1)^{3/2}\right]$$
$$- \frac{k_2(\lambda_2 + 2\mu_2)}{3\alpha_2^2\,q_0\,\eta}\left[1 - \frac{2\alpha_2\,q_0\,\eta\,(L - L_1)}{k_2(\lambda_2 + 2\mu_2)}\right]^{3/2}. \qquad (3.19)$$

We will be mainly interested in the permeabilities, $K_1$ and $K_2$, which depend on $A_1$ and $A_2$, and in the pressure difference, $P_{\text{in}}$-$P_{\text{out}}$, which depends on $A_1$ and $C_1$. The displacements, $u_1$ and $u_2$, depend on $B_1$ and $B_2$, which depend on $A_1$ given by (3.16). Equation (3.11), which is the relation between $q_0$ and $P_{\text{out}}$, becomes

$$P_{\text{in}} - P_{\text{out}} = \frac{(\lambda_1 + 2\mu_1)}{\alpha_1}\left[1 - (1 + 2\alpha_1 A_1)^{1/2}\right], \tag{3.20}$$

where

$$1 + 2\alpha_1 A_1 = -\frac{2\alpha_1 q_0 \eta L_1}{k_1(\lambda_1 + 2\mu_1)}$$
$$+ \left[1 - \frac{\alpha_1}{\alpha_2}\frac{(\lambda_2 + 2\mu_2)}{(\lambda_1 + 2\mu_1)} + \frac{\alpha_1}{\alpha_2}\frac{(\lambda_2 + 2\mu_2)}{(\lambda_1 + 2\mu_1)}\left(1 - \frac{2\alpha_2 q_0 \eta L_2}{k_2(\lambda_2 + 2\mu_2)}\right)^{1/2}\right]^2. \tag{3.21}$$

**3.2.  Permeability and fluid pressure**   The permeability of each mask is obtained from (2.11) and (3.6) as

$$K_n(x) = k_n\left[1 + 2\alpha_n\left(A_n + \frac{q_0 \eta}{k_n(\lambda_n + 2\mu_n)}\,x\right)\right]^{1/2}, \quad n = 1, 2.$$

By using (3.21) for $A_1$ and (3.10) for $A_2$, we find that

$$K_1(x) = k_1\left[-\frac{2\alpha_1 q_0 \eta}{k_1(\lambda_1 + 2\mu_1)}\,(L_1 - x)\right.$$
$$\left. + \left\{1 - \frac{\alpha_1}{\alpha_2}\frac{(\lambda_2 + 2\mu_2)}{(\lambda_1 + 2\mu_1)} + \frac{\alpha_1}{\alpha_2}\frac{(\lambda_2 + 2\mu_2)}{(\lambda_1 + 2\mu_1)}\left(1 - \frac{2\alpha_2 q_0 \eta L_2}{k_2(\lambda_2 + 2\mu_2)}\right)^{1/2}\right\}^2\right]^{1/2} \tag{3.22}$$

for $0 \le x \le L_1$, and

$$K_2(x) = k_2\left[1 - \frac{2\alpha_2 q_0 \eta}{k_2(\lambda_2 + 2\mu_2)}\,(L - x)\right]^{1/2} \tag{3.23}$$

for $L_1 \le x \le L$.

   The fluid pressure is given by (3.8) for $n = 1$ and 2. By using (3.21), (3.10), (3.17) and (3.12) for $A_1, A_2, C_1$ and $C_2$, it can be verified that

$$P_1(x) = P_{\text{in}} - \frac{(\lambda_1 + 2\mu_1)}{\alpha_1}\left[1 - \left\{-\frac{2\alpha_1 q_0 \eta}{k_1(\lambda_1 + 2\mu_1)}\,(L_1 - x)\right.\right.$$
$$\left.\left. + \left(1 - \frac{\alpha_1}{\alpha_2}\frac{(\lambda_2 + 2\mu_2)}{(\lambda_1 + 2\mu_1)} + \frac{\alpha_1}{\alpha_2}\frac{(\lambda_2 + 2\mu_2)}{(\lambda_1 + 2\mu_1)}\left(1 - \frac{2\alpha_2 q_0 \eta L_2}{k_2(\lambda_2 + 2\mu_2)}\right)^{1/2}\right)^2\right\}^{1/2}\right] \tag{3.24}$$

for $0 \le x \le L_1$ and

$$P_2(x) = P_{\text{in}} - \frac{(\lambda_2 + 2\mu_2)}{\alpha_2}\left[1 - \left(1 - \frac{2\alpha_2 q_0 \eta}{k_2(\lambda_2 + 2\mu_2)}\,(L - x)\right)^{1/2}\right] \tag{3.25}$$

for $L_1 \le x \le L$.

The difference between the fluid pressure at the entry at Mask 2, $x = L$, and at the exit at Mask 1, $x = 0$, is given by (3.20). By using again (3.21), the following relation between $q_0$ and the pressure drop $\Delta P$ is obtained:

$$
\begin{aligned}
P_{\text{in}} - P_{\text{out}} &= \Delta P \\
&= \frac{(\lambda_1 + 2\mu_1)}{\alpha_1}\Bigg[1 - \Bigg\{ -\frac{2\alpha_1\, q_0\, \eta\, L_1}{k_1(\lambda_1 + 2\mu_1)} \\
&\quad + \Bigg(1 - \frac{\alpha_1}{\alpha_2}\frac{(\lambda_2 + 2\mu_2)}{(\lambda_1 + 2\mu_1)} + \frac{\alpha_1}{\alpha_2}\frac{(\lambda_2 + 2\mu_2)}{(\lambda_1 + 2\mu_1)}\Bigg(1 - \frac{2\alpha_2\, q_0\, \eta\, L_2}{k_2(\lambda_2 + 2\mu_2)}\Bigg)^{1/2}\Bigg)^2\Bigg\}^{1/2}\Bigg].
\end{aligned}
$$

(3.26)

It is readily verified that (3.26) agrees with (3.24) evaluated at $x = 0$.

The displacement components, $u_1(x)$ and $u_2(x)$, are given by (3.7), where $B_1$ and $B_2$ are given by (3.18) and (3.19). The constants $B_1$ and $B_2$ are expressed in terms of $1 + 2\alpha_1 A_1$ and can be expanded using again (3.21). We will not analyse $u_1(x)$ and $u_2(x)$ since it is sufficient to investigate the properties of the permeability and pressure difference across the double mask to understand the working of the double mask.

### 3.3. Scaling and nondimensionalization

We first introduce scaled physical quantities.

Note that (from (3.23)) the permeability $K_2(x)$ is real for values of $x$ in the range $L_1 \leq x \leq L$, provided

$$
q_0 \leq q_s, \quad \text{where } q_s = \frac{k_2(\lambda_2 + 2\mu_2)}{2\alpha_2\, \eta\, L_2}.
$$

(3.27)

We choose the following scales for the physical variables in both masks:

$$
\text{fluid flux scale} = q_s, \qquad \text{fluid pressure scale } P_s = \frac{\lambda_1 + 2\mu_1}{\alpha_1},
$$
$$
\text{permeability scale} = k_2, \quad \text{length scale} = L.
$$

We emphasize that the scales are not characteristic quantities. They are suitable scales that produce dimensionless variables and give a useful way to present the results. To obtain the actual pressure, for example, we would need to multiply the scaled result by $P_s$.

The scale $q_s$ is the maximum value for the fluid flux in Mask 2, and therefore in the double mask, for given values of $\alpha_2$, $\lambda_2$, $\mu_2$, $k_2$ and $L_2$. It depends only on the parameters and width of Mask 2. The pressure scale $P_s$ is a factor in the pressure difference (3.26) across the double mask. The scale $P_s$ for given values of $\alpha_1$, $\lambda_1$ and $\mu_1$ depends only on the parameters in Mask 1. It is used to scale the pressure in both Mask 1 and Mask 2. The permeability scale, $k_2$, is the permeability of Mask 2 in its undeformed state. The length $L$ is based on the width of the double mask because we are interested, for example, in the pressure difference across the double mask.

We define the following scaled quantities:

$$q_0^* = \frac{q_0}{q_s}, \quad 0 \le q_0^* \le 1,$$

$$x^* = \frac{x}{L} \quad (0 \le x^* \le 1), \quad L_1^* = \frac{L_1}{L}, \quad L_2^* = \frac{L_2}{L}, \quad L_1^* + L_2^* = 1,$$

$$K_1^*(x^*) = \frac{K_1(x)}{k_2}, \quad K_2^*(x^*) = \frac{K_2(x)}{k_2},$$

$$P_1^*(x^*) = \frac{P_1(x)}{P_s}, \quad P_2^*(x^*) = \frac{P_2(x)}{P_s}, \quad \Delta P^* = \frac{\Delta P}{P_s}.$$

From (3.22) and (3.23), the scaled permeabilities in Mask 1 and Mask 2 are

$$K_1^*(x^*) = \frac{k_1}{k_2} \left[ \left\{ 1 - \frac{\alpha_1}{\alpha_2} \frac{(\lambda_2 + 2\mu_2)}{(\lambda_1 + 2\mu_1)} + \frac{\alpha_1}{\alpha_2} \frac{(\lambda_2 + 2\mu_2)}{(\lambda_1 + 2\mu_1)} (1 - q_0^*)^{1/2} \right\}^2 \right.$$
$$\left. - \frac{\alpha_1}{\alpha_2} \frac{(\lambda_2 + 2\mu_2)}{(\lambda_1 + 2\mu_1)} \frac{k_2}{k_1} q_0^* \frac{(L_1^* - x^*)}{(1 - L_1^*)} \right]^{1/2} \tag{3.28}$$

for $0 \le x^* \le L_1^*$, and

$$K_2^*(x^*) = \left[ 1 - q_0^* \frac{(1 - x*)}{(1 - L_1^*)} \right]^{1/2} \tag{3.29}$$

for $L_1^* \le x^* \le 1$. From (3.26), the scaled pressure difference across the double mask is

$$\Delta P^\star = 1 - \left[ \left\{ 1 - \frac{\alpha_1}{\alpha_2} \frac{(\lambda_2 + 2\mu_2)}{(\lambda_1 + 2\mu_1)} + \frac{\alpha_1}{\alpha_2} \frac{(\lambda_2 + 2\mu_2)}{(\lambda_1 + 2\mu_1)} (1 - q_0^*)^{1/2} \right\}^2 \right.$$
$$\left. - \frac{\alpha_1}{\alpha_2} \frac{(\lambda_2 + 2\mu_2)}{(\lambda_1 + 2\mu_1)} \frac{k_2}{k_1} q_0^* \frac{L_1^*}{(1 - L_1^*)} \right]^{1/2}. \tag{3.30}$$

Equation (3.30) is a relation between $q_0^*$ and $\Delta P^*$: only one of $q_0^*$ and $\Delta P^*$ can be specified. The other is obtained from (3.30).

The fluid pressure is continuous across the interface $x = L_1$, and it is readily verified from (3.24) and (3.25) that $P_1(x)$ for $0 \le x \le L_1$ and $P_2(x)$ for $L_1 \le x \le L$ are increasing functions of $x$. The quantity of interest is the pressure difference (3.26) across the double mask. We will therefore not investigate $P_1(x)$ and $P_2(x)$ in each mask separately, and therefore we do not write $P_1(x)$ and $P_2(x)$ in scaled form.

The results will be fully analysed in Section 4. We give here a few elementary properties of the solutions. From (3.28) and (3.29),

$$\frac{dK_1^*}{dx^*} = \frac{1}{2} \frac{\alpha_1}{\alpha_2} \frac{(\lambda_2 + 2\mu_2)}{(\lambda_1 + 2\mu_1)} \frac{k_1}{k_2} \frac{q_0^*}{K_1^*(x^*)(1 - L_1^*)} > 0, \quad 0 \le x^* \le L_1^*,$$

$$\frac{dK_2^*}{dx^*} = \frac{q_0^*}{2K_2^*(x^*)(1 - L_1^*)} > 0, \quad L_1^* \le x^* \le 1. \tag{3.31}$$

Hence, $K_1^*(x^*)$ and $K_2^*(x^*)$ are increasing functions of $x^*$. In general, the permeabilities $K_1^*(x^*)$ and $K_2^*(x^*)$ will not be equal at the interface $x^* = L_1^*$. It can be verified that

$$K_1^*(L_1^*) = K_2^*(L_2^*) \tag{3.32}$$

provided

$$q_0^* = \frac{\left(1 - \dfrac{k_1}{k_2}\right)\left(1 + \dfrac{k_1}{k_2} - \dfrac{2k_1}{k_2}\dfrac{\alpha_1}{\alpha_2}\dfrac{(\lambda_2 + 2\mu_2)}{(\lambda_1 + 2\mu_1)}\right)}{\left(1 - \dfrac{k_1}{k_2}\dfrac{\alpha_1}{\alpha_2}\dfrac{(\lambda_2 + 2\mu_2)}{(\lambda_1 + 2\mu_1)}\right)^2} \tag{3.33}$$

and

$$\frac{k_1}{k_2}\frac{\alpha_1}{\alpha_2}\frac{(\lambda_2 + 2\mu_2)}{(\lambda_1 + 2\mu_1)} \neq 1.$$

When

$$\frac{\alpha_1}{\alpha_2}\frac{(\lambda_2 + 2\mu_2)}{(\lambda_1 + 2\mu_1)} = \frac{k_2}{k_1},$$

(3.32) is satisfied for all $0 \leq q_0^* \leq 1$ provided $k_1 = k_2$.

From (3.31) and (3.33),

$$
\begin{aligned}
K_1^*(0) &= \frac{k_1}{k_2}\,[F^2(q_0^*) - G(q_0^*)]^{1/2}, \\
\Delta P^* &= 1 - [F^2(q_0^*) - G(q_0^*)]^{1/2},
\end{aligned}
\tag{3.34}
$$

where

$$F(q_0^*) = 1 - \frac{\alpha_1}{\alpha_2}\frac{(\lambda_2 + 2\mu_2)}{(\lambda_1 + 2\mu_1)} + \frac{\alpha_1}{\alpha_2}\frac{(\lambda_2 + 2\mu_2)}{(\lambda_1 + 2\mu_1)}\,(1 - q_0^*)^{1/2}, \tag{3.35}$$

$$G(q_0^*) = \frac{\alpha_1}{\alpha_2}\frac{(\lambda_2 + 2\mu_2)}{(\lambda_1 + 2\mu_1)}\frac{k_2}{k_1}\,q_0^*\,\frac{L_1^*}{(1 - L_1^*)}, \tag{3.36}$$

and

$$F(0) = 1, \quad G(0) = 0. \tag{3.37}$$

From (3.37) and (3.34),

$$\Delta P^* = 1 - \frac{k_2}{k_1}\,K_1^*(0). \tag{3.38}$$

The pressure difference $\Delta P^*$ and the permeability $K_1^*(0)$ which are related through (3.38) are important scaled quantities in the understanding of the working of the double mask and are fully analysed in terms of the functions $F^2(q_0^*)$ and $G(q_0^*)$ in Section 4.

**3.4. Parameter reduction** The dimensionless parameters involved are the zero flow permeability ratio $k_1/k_2$, the "compressibility" ratio $\alpha_1/\alpha_2$, the elastic modulus ratio $(\lambda_1 + 2\mu_1)/\lambda_2 + 2\mu_2)$ and the filter thickness ratio $L_1^*/(1 - L_1^*)$. However, an examination of the results in Section 3.3 indicates that the compressibility and elastic parameters only occur in combination leaving just three dimensionless groups:

$$\Lambda_{21} = \frac{(\lambda_2 + 2\mu_2)/\alpha_2}{(\lambda_1 + 2\mu_1)/\alpha_1}, \quad k_{21} = \frac{k_2}{k_1}, \quad L_{12}^* = \frac{L_1^*}{1 - L_1^*}.$$

The implication of this observation is that a changed flow behaviour can be achieved by either adjusting the permeability parameters $\alpha_i$ or by adjusting the elastic parameters $\lambda_i + 2\mu_i$. In terms of this new set of parameters, the expressions for the scaled permeabilities are given by

$$K_1^*(x^*) \equiv \frac{K_1(x^*)}{k_2} = \frac{1}{k_{21}}\sqrt{F^2(q_0^*) - G^*(q_0^*, x^*)},$$

$$K_2^*(x^*) \equiv \frac{K_2(x^*)}{k_2} = \sqrt{1 - q_0^*\left(\frac{1 - x^*}{1 - L_1^*}\right)}$$

with

$$G(q_0^*, x^*) = k_{21}\Lambda_{21}\, q_0^* L_{12}^*(x^*), \quad L_{12}^*(x^*) = \left(\frac{L_1^* - x^*}{1 - L_1^*}\right).$$

The scaled pressure difference is given by

$$\Delta P^* = 1 - [F^2(q_0^*) - G(q_0^*, 0)]^{1/2}$$

with

$$G(q_0^*, 0) = G(q_0^*) = k_{21}\,\Lambda_{21}\, q_0^* L_{12}^*, \quad F(q_0^*) = 1 - \Lambda_{21}\,(1 - (1 - q_0^*)^{1/2}).$$

It is useful to think of the above results as determining the (scaled) pressure drop $\Delta P^* > 0$ required to drive a prescribed flow $q_0^*$ through the two masks under steady-state conditions.

## 4. Compressible double mask results

It is easier to solve the problem of two masks in the incompressible (constant permeability) mask case directly than to take the small compressibility limit in the general case, so we have relegated this work to Appendix A. A few of the results in this case are however worth noting. In a double mask with constant permeabilities, the pressure drop required to drive flux $q_0$ through the mask is given by (A.1), which can be written in the more understandable (unscaled) form

$$\Delta P = q_0\,\eta\left[\frac{L_2}{k_2} + \frac{L_1}{k_1}\right];$$

we have two resistances in series determining the through-flow. Note that the through-flux increases in direct proportion to the applied pressure drop, so that there is no upper bound on the through-flux in the incompressible masks case; we will see that for compressible masks, there is an upper bound. Note also that the pressure is continuous through the masks but the permeability is discontinuous across the interface between the filters.

For compressible filters, there are two primary dimensionless parameters governing the flow behaviour: the zero flux permeability ratio $k_{21}$ and the poroelastic ratio parameter $\Lambda_{21}$. In the covid mask context, it is sensible to have $k_{21} \geq 1$ so that larger particles are filtered out by the filter closest to the face; we will assume this is the case for the simulations. The results we obtain are not obvious so before undertaking an analysis of the general situation, it is useful to plot out some steady-state solutions corresponding to fixed values of the zero flux permeability ratio $k_{21}$.

### 4.1.  Preliminary simulations

*4.1.1. The $k_{21} = 1, \Lambda_{21} = 1$ case*  Note that this case includes the case in which both filters are identical, which we will refer to as the single-filter case, but also includes cases with different values of $\alpha$ but compensating values of $\lambda + 2\mu$ arranged so that the poroelastic parameter ratio $\Lambda_{21}$ remains unchanged; this feature may be significant in terms of mask design.

Plots of permeability through the mask (two filters) are displayed in Figure 2. We note that for zero flux conditions, compressibility effects disappear and the scaled permeability $K^*(x) = 1$, as required by the scaling. As influx $q_0^*$ levels increase from zero, the permeability decreases uniformly according to our poroelastic model under the mask compression circumstances

$$\Delta P^* = P_{\text{in}}^* - P_{\text{out}}^* > 0$$

of interest here.

This particular parameter set is special in that the (local) permeability is continuous through the mask; for all other parameter combinations, there is a discontinuity across the interface $x^* = L_1^*$ between the two filters. The reader will recall that the external face of the mask ($x = 0$) is rigidly constrained by a porous grid, so that the compression is greatest here and thus the permeability $K^*(x)$ reaches a minimum at $x^* = 0$ and increases with distance from this outer mask face, as seen in Figure 2.

Of course no steady-state solution is possible if the permeability is zero anywhere within the mask, and the first location to realise such a zero flux state is the external face of the mask $x^* = 0$. Once this happens the flow "shuts down", so that there is an abrupt change in through-flux from a maximum value (of $q_0^* = 0.5$ for our present set of parameters, as seen in Figure 2) to zero. Higher steady-state flux levels than this maximum value are not possible basically because the pores in filter 1 have closed. Of course a higher pressure drop than $\Delta P^* = 1$ can be applied to the mask, but the excess pressure will simply be taken up elastically by the filter fibres.
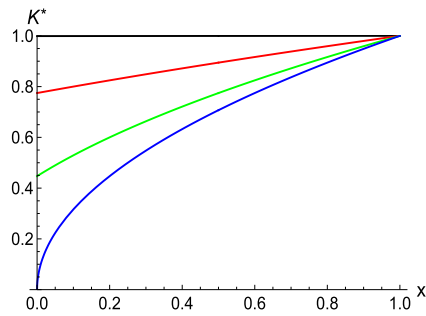
FIGURE 2. The $k_{21} = 1$, $\Lambda_{21} = 1$ single-mask case. Local permeability variations $K^*(x)$ through the mask for increasing through-flux levels: $q_0^* = 0$ (top, black), then 0.2 (red), 0.4 (green), 0.5 (lowest, blue). The maximum possible (scaled) flux through the mask is $q_0^* = 0.5$ corresponding to the blue curve.
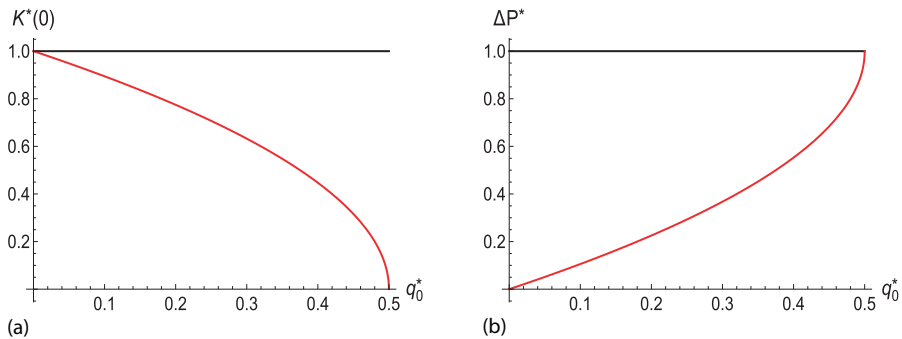


(a)                                                              (b)

FIGURE 3. The $k_{21} = 1$, $\Lambda_{21} = 1$ single-mask case: (a) Global permeability versus flux results. Note that zero global permeability occurs with a maximum through-flux of $q_0^* = 0.5$. Note that the permeability is continuous across the interface ($x = 0.5$) in this special case. (b) Pressure drop versus flux results. Note that the maximum pressure drop $\Delta P^* = 1$ occurs when the through-flux is maximal at $q_0^* = 0.5$.

The mask consisting of the two filters can be thought of as an equivalent single mask with effective global (or bulk) permeability defined by the pressure drop across the two filters verses through-flux relation, which is determined by $K^*(0)$, see (3.38). This effective global permeability will be dependent on the through-flux and will vary from $K^*(0) = 1$ when $q_0^* = 0$ to $K^*(0) = 0$ when $q_0^* = 0.5$, see Figure 3(a). The associated pressure drop verses flux relation is shown in Figure 3(b); the maximal pressure drop ($\Delta P^* = 1$) is realized with a through-flux of $q_0^* = 0.5$. It should be noted that a mask consisting of a single filter (just filter 2) would allow the maximal through-flux $q_0^* = 1$, the thickness of the single-layer mask being half that of the double mask.

*4.1.2. The $k_{21} = 1$, $\lambda_{21} \neq 1$ case*  Note the abrupt drop in the (local) permeability $K^*(x)$ across the interface (here at $x = 0.5$) between the two layers in the case when $\lambda_{21} = 2$; see Figure 4(a). Flux shut down now occurs at a lower maximum flux level compared with the $\Lambda_{21} = 1$ case of $q_0^* = 0.26 < 0.5$ due to the increase in the
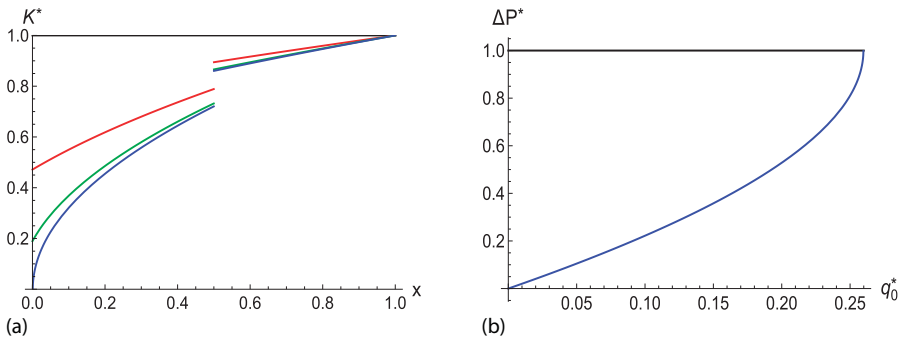
FIGURE 4. The $k_{21} = 1$, $\Lambda_{21} = 2$ case. (a) Local permeability variations through the mask for increasing through-flux levels: $q_0^* = 0$ top (black) curve, then 0.2 (red), 0.25 (green), 0.26 (blue, lowest). A (scaled) maximum flux level of $q_0^* = 0.26$ is possible (blue curve). (b) The associated pressure drop versus flux relationship.
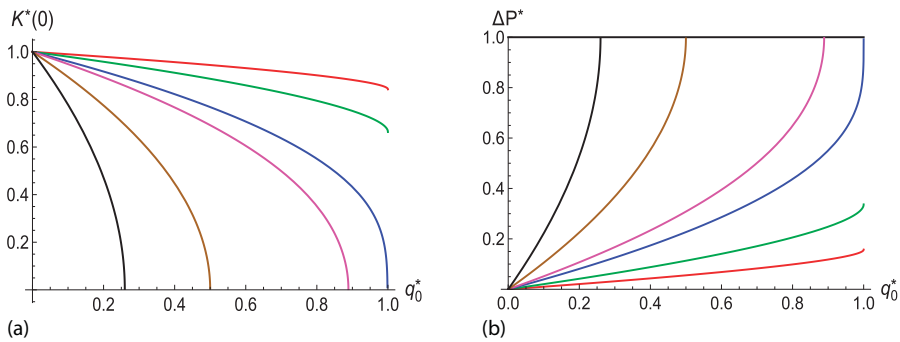


FIGURE 5. The $k_{21} = 1$, $\Lambda_{21}$ variable case. (a) Global permeability verses flux results for $\Lambda_{21} = 0.1$ (top, red), then 0.2 (green), 0.38 (blue) $\cdots$ 2.0 (bottom, black). (b)The pressure drop verses flux relationship for $\Lambda_{21} = 0.1$ (bottom, red), then 0.2 (green), 0.38 (blue), $\cdots$ 2 (top, black). The blue curve with $\Lambda_{21} = 0.38$ separates out the two possible scenarios.

poroelastic ratio. The associated pressure drop versus flux relationship is shown in Figure 4(b). Again, shut down is abrupt; flux levels reduce to zero if the pressure drop exceeds the maximal value $\Delta P^* = 1$.

The effect of varying the poroelastic parameter ratio $\Lambda_{21}$ (with $k_{21} = 1$) on the permeability and pressure drop is shown in Figure 5. There are two distinctly different cases.

(1) Either curves hit the maximal flux value of the $q^* = 1$ barrier. This occurs for smaller poroelastic ratio situations ($\Lambda_{21} = 0.1$ (red), 0.2 (green)). Note that $q^* = 1$ corresponds to an unscaled flux value of

$$q_s = \frac{k_2(\lambda_2 + 2\mu_2)}{2\alpha_2 \, \eta \, L_2};$$

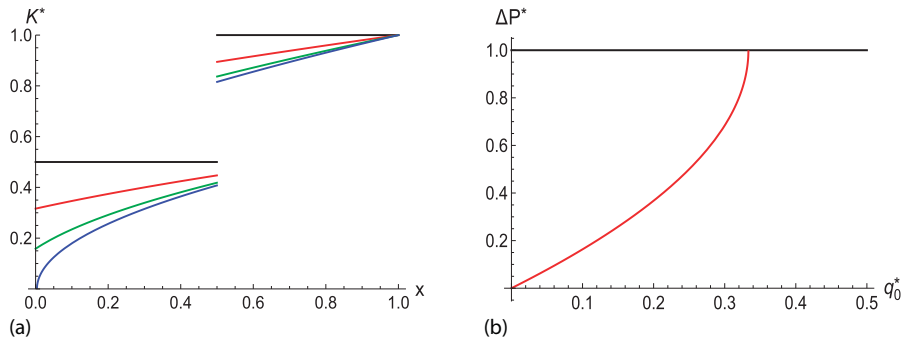it is mask 2 (the inner mask) that controls the limiting behaviour.

FIGURE 6. The $k_{21} = 2$, $\Lambda_{21} = 1$ case. (a) (Local) permeability variations through the mask for increasing through-flux levels varying from zero to cut-off ($q_0^* = 0$ (top, black), then 0.2 (red), 0.3 (green), 0.335 (bottom, blue)). Cut off occurs at a flux level of $q_0^* = 0.334$ (the blue curve). (b) The pressure drop verses flux relationship.
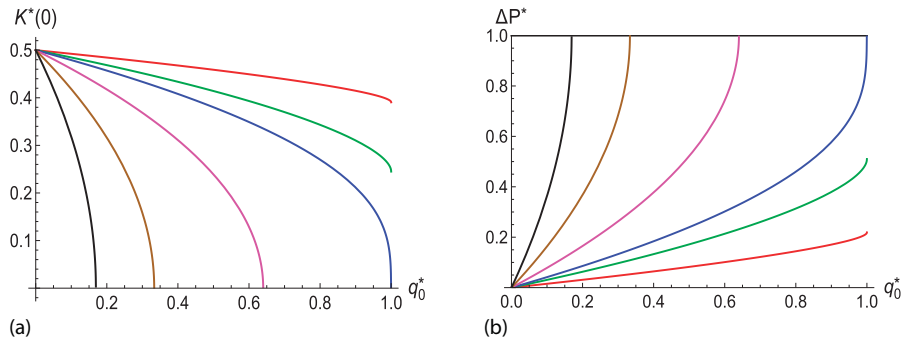


FIGURE 7. The $k_{21} = 2$, $\Lambda_{21}$ variable case. (a) Global permeability verses flux results for $\Lambda_{21} = 0.1$ (top, red), then 0.2 (green), 0.27 (blue), 0.5 (magenta), 1 (brown), 2 (bottom, black). (b) The pressure drop verses flux relationship for the same $\Lambda_{21}$ range; $\Lambda_{21} = 0.1$ (bottom, red) etc.. The (blue) $\Lambda_{21} = 0.27$ case separates out the two possible scenarios.

(2) Or curves hit the maximal pressure drop barrier $\Delta P^* = 1$. This occurs for poroelastic values larger than $\Lambda_{21} = 0.38$. Note that this corresponds to a real (unscaled) pressure drop of $(\lambda_1 + 2\mu_1)/\alpha_1$; it is mask 1 (the outer mask) that controls the limiting behaviour.

The blue curve, corresponding to $\Lambda_{21} = 0.38$, separates the two cases.

*4.1.3. The $k_{21} = 2$ case* Qualitatively, the results in the $k_{21} = 2$ case are similar to those obtained with $k_{21} = 1$. First, we present the $\Lambda_{21} = 1$ case (see Figure 6). The maximum possible flux is $q_0^* = 0.335 < 1$ which results if a maximal pressure drop of $\Delta P^* = 1$ is applied.

The results for variable poroelastic ratios ($\Lambda_{21}$) are displayed in Figure 7.
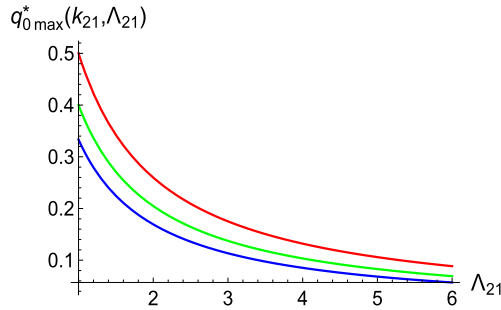
FIGURE 8. Maximal flux levels for two masks as a function of $\Lambda_{21}$ for fixed values of $k_{21} = 1$ (top, red), then $k_{21} = 1.5$ (green) and $k_{21} = 2$ (bottom, blue).

*4.1.4. Maximal through-flux levels* We have seen that through-flux levels are reduced by increases of either the zero flux permeability factor $k_{21}$ or the poroelastic parameter $\Lambda_{21}$. This may be useful for design purposes, so the dependence of the maximum flux possible through the two masks as a function of the two parameters is of interest. We can obtain this by the equation $K^*(0) = 0$ and solving for $q_0^*$. Exact (but complicated) results are obtained and are plotted in Figure 8. Note that reduced maximum flux levels occur for larger values of $\Lambda_{21}$. Evidently, the same maximum flux result can be obtained for a prescribed $k_{21}$ by adjusting $\Lambda_{21}$, as seen in Figure 8.

**4.2. The general solution structure** As noted earlier, real steady-state solutions for mask flow exist in the range given by $q_0^* \leq 1$ and $\Delta P^* \leq 1$, otherwise the permeability goes to zero or becomes complex, indicating that no steady-state flow is possible. In terms of the solution components $(F^2, G)$ defined by (3.35) and (3.36), real values for the pressure drop only exist if $F^2 \geq G$. When $F^2 = G$, the scaled pressure reaches its maximal value of $P^* = 1$, with a global permeability of $K_1^*(0) = 0$. With this in mind, we plot in Figure 9 the functions $F^2(q_0^*)$ and $G(q_0^*)$ for a range of values of the poroelastic parameters $k_{21}$ and $\Lambda_{21}$. Note that $G(q_0^*)$ is a linear function of $q_0^*$, whereas $F^2(q_0^*)$ can either curve upwards or downwards depending on the values of the zero flux permeability ratio $k_{21}$ and the poroelastic ratio $\Lambda_{21}$. This means that, over the allowable flux range $0 \leq q_0^* \leq 1$, there will be for $F^2(q_0^*) - G(q_0^*) = 0$ either no solutions, one solution or two solutions for $q_0^*$, depending on the poroelastic parameter values.

In Figure 9, we plot $G$ and $F^2$ for a conductivity ratio $k_{21} = 1$, and a range of values of the poroelastic ratio $\Lambda_{21}$. For increasing values of $\Lambda_{21}$, the $F^2$ and $G$ curves first cross at $q_0^* = 1$ so that a transition between the different solution structures can be determined by equating $F^2(1)$ to $G(1)$. This gives the result that, if the thickness adjusted permeability ratio $k_{21}(L_1^*/(1 - L_1^*))$ is greater than the critical value

$$k_{21}^{\text{crit}}(\Lambda_{21}) = \frac{(1 - \Lambda_{21})^2}{\Lambda_{21}}, \tag{4.1}$$

then there is just one solution for $q_0^*$ (given by $q_0^* = 0.126$ in the $k_{21} = 1$ case). The critical $k_{21}$ curve is plotted in Figure 10. Above this curve (the shaded region), there
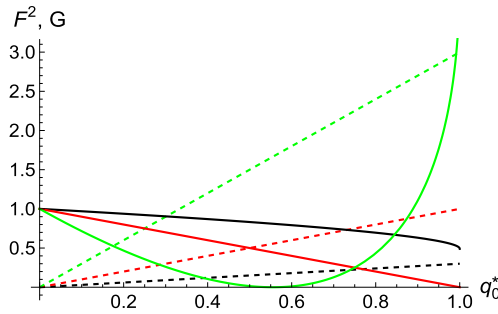
FIGURE 9. Plots for $F^2(q_0^*, k_{21}, \Lambda_{21})$ (solid curves) and $G(q_0^*, k_{21}, \Lambda_{21})$ (dashed curves) for $k_{21} = 1$, and $\Lambda_{21} = 0.3$ (black), 1 (red) and 3 (green). The curves for $\Lambda_{21} = 0.3$ (black) do not intersect. Those for $\Lambda_{21} = 1$ (red) intersect at one point. Those for $\Lambda_{21} = 3$ (green) intersect at two points.
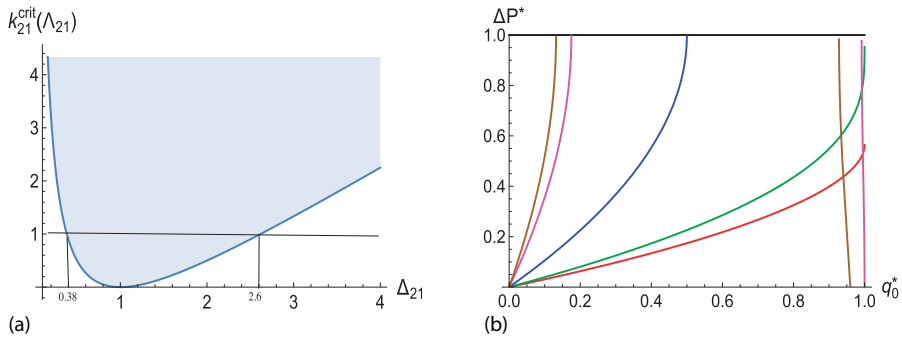


(a)                                                        (b)

FIGURE 10. The critical $k_{21}$ curve ($k_{21}^{crit}(\Lambda_{21})$) given by (4.1) and solution branches in the $L_1^* = 1/2$ case. (a) The critical curve splits the parameter space into three regions (left, above and right). (b) Solution curves corresponding to $k_{21} = 1$. The red curve (with $\Lambda_{21} = 0.3$) is in the small lambda range, the blue curve ($\Lambda_{21} = 1$) is in the medium lambda range, with the green curve ($\Lambda_{21} = 0.38$) splitting the two solution zones. The (two) magenta curves correspond to ($\Lambda_{21} = 3$) are in the large lambda range.

is just one solution for $q_0^*$, to the left of this critical curve, there are no solutions, while to the right, there are two solutions. In the case in which $k_{21} = 1$, the regions are defined by the small lambda range $(0, 0.38)$, the medium range $(0.38, 2.6)$ and the high lambda range $> 2.6$, see Figure 10(a). The associated $\Delta P^*(q_0^*)$ solution curves are displayed in Figure 10(b). In the small lambda range, there is a single solution (the red curve) with flux levels increasing in response to the pressure drop $\Delta P^*$ until the maximum through-flux of $q_0^* = 1$ is reached (asymptotically) with $\Delta P^* < 1$; the maximum possible pressure drop is not reached. In the medium lambda range, there is a single solution (shaded region blue curve) with flux levels increasing with the applied pressure drop until this reaches its maximal value $\Delta P^* = 1$, with a value of $q_0^*$ less than its maximal value of unity. As described earlier, shut down occurs for higher pressure drops. This medium lambda range includes the $k_{21} = 1$, $\Lambda_{21} = 1$ single-filter case. In the large lambda range ($\Lambda_{21} = 3$ (magenta)), there are two solution branches.
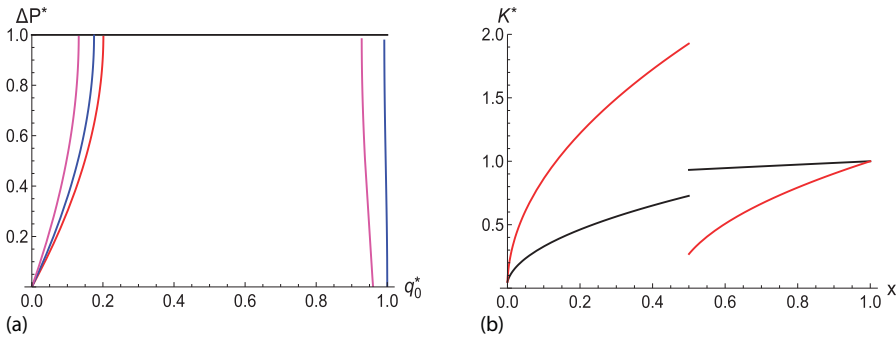
FIGURE 11. Two possible solutions in the large $\Lambda_{21}$ case with $k_{21} = 1$. (a) $\Delta P^*(q_0^*)$. The red curve corresponds to $\Lambda_{21} = 2.6$ which lies on the critical curve so there is just one branch. The blue curve ($\Lambda_{21} = 3$) and magenta ($\Lambda_{21} = 4$) curves correspond to $\Lambda_{21} > 2.6$; there are two branches. (b) Local permeability variations through the mask for the two possible solution branches with $\Lambda_{21} = 4$. The black curves (left bottom and right top with $q_0^* = 0.126$) correspond to the normal (small $q_0^*$) branch, the red curves (left top and right bottom with $q_0^* = 0.929$) to the large flux branch.

Examples of solutions in the small and medium lambda range have been described before. All these solutions continuously evolve from an initial no flow $(\Delta P^*, q_0^*) = (0, 0)$ state. The small $q_0^*$ branch in the large lambda case also evolves from an initial no flow state, but the second (large $q_0^*$) branch does not connect onto this zero flux state. In Figure 11(a), we have plotted pressure drop versus flux results in the $k_{21} = 1$ case with $\Lambda_{21} = 2.6$, 3 and 4 (the large lambda range). Note that $\Lambda_{21} = 2.6$ lies on the border of the large/medium parameter range and there is a single solution branch (the red curve) which matches the solutions in the neighbouring medium lambda parameter range. For larger values of $\Lambda_{21}$, a second (large $q_0^*$) branch opens up (the blue curve), indicating that under steady-state circumstances, the same pressure drop can result in either a small or a large through-flux. Evidently, the flow behaviour through the mask will be different in the two cases.

Figure 11(a) displays the pressure drop versu flux relation for $\Lambda_{21}$ values close to the transitional value of $\Lambda_{21} = 2.6$ (red curve). One can see the two branches (blue, magenta) opening up for $\Lambda_{21} = 3$ and 4; both branches move to the left as $\Lambda_{21}$ increases.

To examine this second branch situation further, we determine permeability variations through the mask for the two solutions corresponding to a pressure drop of $\Delta P^* = 0.951$ close to maximal pressure drop of unity. The corresponding flux levels are $q_0^* = 0.131$ and $q_0^* = 0.928$. The results for the (local) permeability variations through the masks are displayed in Figure 11(b). In the (normal) small lambda branch case (the black curve), the variations in permeability within filter 2 are moderate with larger variations through the external filter 1, whereas in the large $q_0^*$ branch, there are large variations in permeability through both filters. As indicated earlier, the small flux branch results from a (gradual) increase in pressure drop from zero, so this is indeed the situation one would normally expect. If, however, the pressure drop across the mask

is at its maximal value of unity (and so is "at" shut down), then the through-flux may either be at a maximal value or zero, and a small change in the applied pressure may cause the solution to switch branches.

In explanation, the external pressure drop on the mask can be either taken up in filter 1 fibres or filter 2 fibres, and what happens depends on history. A slow build up in pressure forcing will likely result in the low flux solution whereas an abrupt pressure change will compress filter 2 before filter 1 responds, giving rise to the high-flux result.

## 5. Summary and observations

The objective of this work was to assess the benefits of using a mask with two compressible filters, and we focused our attention on the steady-state flow-through behaviour under flow out conditions. Of particular interest was the effect of filter compressibility on the flow-through behaviour. The thought was that using two filters may make it possible to design a mask that is both comfortable under normal breathing conditions (allowing relatively free exchange of air) and yet relatively impermeable under high flux expulsion (sneezing) conditions. The results we obtained showed that the reduction in permeability required to produce this changed behaviour could be achieved using either a single filter compressible mask or by using two filters with different poroelastic parameters. However, a more dramatic change in behaviour is possible using two filters, and the poroelastic parameters can be more easily adjusted. A required behaviour can be achieved by either adjusting the permeability ratio param-eter and/or the poroelastic ratio parameter and/or the filter thickness parameter, so there is considerable flexibility (at least theoretically) available for the design engineer.

Some features of model results require further thought. We have seen that the effect of compressibility on the flow behaviour for both a single mask or two masks is dramatic. Whereas in the incompressible mask/s case there is no upper bound on the through-flux, in the compressible single- and two-mask cases, there is an upper limit. In the two-mask case, this limit is given by

$$q_s = \frac{k_2(\lambda_2 + 2\mu_2)}{2\alpha_2 \eta L_2},$$

which is determined by the poroelastic parameters of the near face *inner* filter *only*. This maximum flux possibility will only be realized, however, with increasing applied pressure drop if the *outer* filter does not shut down the flow before such flux levels are reached. This will occur if pressure drop levels reach the critical value of

$$P_s = \frac{\lambda_1 + 2\mu_1}{\alpha_1};$$

again determined *only* by the poroelastic parameters of the *outer* mask. It is this second scenario that is desirable in the covid mask context; we would like the outer mask to trap all particles under sufficiently high-pressure sneeze or cough circumstances. Under such circumstances, a maximum flux less than the $q_s$ will be realized when the

pressure reaches $P_s$, and if a higher pressure drop is applied, then the flow will cease entirely with the pressure taken up in the solid matrix. In addition to all this, there is a third possible high-pressure scenario predicted by our model.

All the above scenarios are based on a *linear* poroelastic model (2.11) which is not likely to apply at near pore closure (zero permeability) conditions. The filters consist of pores of different sizes, and so the effect of increasing compression close to cut-off conditions will be to cause the smaller pores to first close up but leaving the larger pores open and thus allowing some reduced through-flow; evidently a nonlinear permeability versus displacement relationship will result. It seems unlikely that detailing this nonlinear behaviour is necessary in context; a "dribbling flow" is for all practical purposes "no flow". As indicated in the main text, the third scenario corresponds to the situation of a garden hose under high pressure with the hose valve almost closed; unstable oscillations may occur. Again, in context, this is not likely to be a real issue.

Typically more sophisticated masks such as the N-95 have a thin inner layer to absorb moisture and a thin outer water repellent layer to reject moisture. That is in addition to the one or more filtering layers. Assuming these layers are incompressible and thin, the above theory goes through with minor modifications to pressure drop across the filters.

Future work will address the particle filtering issues.

## Appendix A. Incompressible double masks

It is easier to solve the problem of two masks with constant permeability directly than to take the limit of two compressible masks. The governing equations are (2.9), (2.10) with $K_n = k_n$ = constant, and (2.13), subject to the boundary conditions (2.14), (2.15) and (2.16) and to the matching conditions (2.17), (2.18) and (2.19). Since the permeability is constant for each mask we solve for the displacements $u_1(x)$ and $u_2(x)$.

For Mask 1,

$$K_1 = k_1,$$

$$u_1(x) = -\frac{q_0 \eta}{2k_1(\lambda_1 + 2\mu_1)} x \left[ 2\left(L_1 + \frac{k_1}{k_2} L_2\right) - x \right],$$

$$P_1(x) = P_{\text{in}} - \frac{q_0 \eta L_2}{k_2} \left[ 1 + \frac{k_2}{k_1} \frac{(L_1 - x)}{L_2} \right],$$

where $0 \le x \le L_1$.

For Mask 2,

$$K_2 = k_2,$$

$$u_2(x) = u_1(L_1) - \frac{q_0 \eta}{2k_2(\lambda_2 + 2\mu_2)} (x - L_1)(L_1 + 2L_2 - x),$$

$$P_2(x) = P_{\text{in}} - \frac{q_0 \eta}{k_2} (L - x),$$

where $L_1 \leq x \leq L$ and

$$u_1(L_1) = -\frac{q_0\,\eta\,L_1}{2k_1(\lambda_1 + 2\mu_1)}\left(L_1 + \frac{2k_1}{k_2}\,L_2\right) < 0.$$

Also the pressure difference satisfies

$$\Delta P = P_{\text{in}} - P_{\text{out}} = \frac{q_0\,\eta\,L_2}{k_2}\left[1 + \frac{k_2}{k_1}\,\frac{L_1}{L_2}\right], \tag{A.1}$$

which is also the relation between $P_{\text{out}}$ and $q_0$.

Although the permeability is constant, the masks can deform and we see that for the displacement, $u_1(x) < 0$ for $0 \leq x \leq L_1$ and $u_2(x) < 0$ for $L_1 \leq x \leq L$.

Both $P_1(x)$ and $P_2(x)$ are increasing functions of $x$ and the pressures match at the interface $x = L_1$. The pressure $P_2(x) \geq 0$ for all $L_1 \leq x \leq L$ provided

$$q_0 \leq \frac{P_{\text{in}}\,k_2}{\eta\,L_2},$$

while $P_1(x) \geq 0$ for all $0 \leq x \leq L_1$ provided

$$q_0 \leq \frac{P_{\text{in}}\,k_2}{\eta\,L_2\,\{1 + (k_2/k_1)(L_1/L_2)\}}. \tag{A.2}$$

Equation (A.2) follows directly from (A.1) and is the condition for $P_{\text{out}} \geq 0$. Unlike the maximum fluid flux $q_s$ given by (3.27) for the permeability $K_2(x)$ of the double compressible mask to be real, the flux (A.2) is independent of the effective Lamé constants, $\lambda_2 + 2\mu_2$, and depends on the pressure $P_{\text{in}}$.

We do not introduce scaled variables, because we are focusing on compressibility effects on the permeability and they are absent in the double mask with constant permeabilities.

## Acknowledgements

*Graeme Hocking*: For many years, we have worked with Graeme on many problems, as have our many good friends and colleagues from Australia, New Zealand, Ireland, U.K., South Africa and elsewhere. It has been a gift to work with Graeme both

professionally and as a friend. In his characteristically quiet way, he does *really* worthy things.

Thank you Graeme.

# References

[1]   T. Dbouk and D. Drikakis, "On respiratory droplets and face masks", *Phys. Fluids* **32** (2020) Article ID 063302, 1–11; doi:10.1063/5.0015044.

[2]   A. Fauci, CNBC, 26 January 2021; https://www.cnbc.com/2021/01/25/dr-fauci-double-mask-during-covid-makes-common-sense-more-effective.html.

[3]   N. D. Fowkes, "Covid-19 mask design", in: *Proceedings of the South African mathematics in industry study group 2021* (ed. D. P. Mason) (University of Witwatersrand, Johannesburg, South Africa, 2023). https://www.wits.ac.za/events-archive/conferences/mathematics-in-industry-study-group/past-conferences/misg-2021/.

[4]   P. Howell, G. Kozyreff and J. Ockendon, *Applied solid mechanics* (Cambridge University Press, Cambridge, 2009) 408–412.

[5]   J. Köry, A. U. Krupp, C. P. Please and I. Griffiths, "The effect of compressibility on the behaviour of filter media", *IMA J. Appl. Math.* **85** (2020) 564–583; doi:10.1093/imamat/hxaa018.

[6]   R. T. Ogulata, "Air permeability of Woven Fabrics", *J. Text. Appar. Technol. Manag.* **5** (2006) 1–10; doi:10.4172/2329-9568.S1-005.

[7]   K. Parker, R. Mehta and C. Caro, "Steady flow in porous elastically deformable materials", *J. Appl. Mech.* **54** (1987) 794–800; doi:10.1115/1.3173119.

[8]   M. Rajat, K. Breuer and J. H. Seo, "The flow physics of face masks", *Annu. Rev. Fluid Mech.* **55** (2023) 193–211; doi:10.1146/annurev-fluid-120720-035029.